BIOCHEMISTRY
including biophysical chemistry & molecular biology

Article

pubs.acs.org/biochemistry

Locked on One Side Only: Ground State Dynamics of the Outer Membrane Efflux Duct TolC

Martin Raunest and Christian Kandt*

Computational Structural Biology, Department of Life Science Informatics B-IT, Life and Medical Sciences Center, University of Bonn, Dahlmannstrasse 2, 53113 Bonn, Germany

Supporting Information

ABSTRACT: Playing a major role in the expulsion of antibiotics and the secretion of cell toxins in conjunction with inner membrane transporters of three protein superfamilies, the outer membrane channel TolC occurs in at least two states blocking or permitting the passage of substrates. The details of the underlying gating mechanism are not fully understood. Addressing the questions of extracellular access control and periplasmic gating mechanism, we conducted a series of independent, unbiased 150−300 ns molecular dynamics simulations of wild-type TolC in a phospholipid membrane/150 mM NaCl water environment. We find that TolC opens and closes freely on the extracellular side, suggesting the absence of a gating mechanism on this side in the isolated protein. On the periplasmic side, we observe the outer periplasmic bottleneck region adopting in all simulations a conformation more open than the TolC wild-type crystal structures until in one run the successive binding of two sodium ions induces the transition to a conformation more closed than any of the available TolC X-ray structures. Concurrent with a heightened sodium residence probability near Asp374, the inner periplasmic bottleneck region at Asp374 remains closed throughout the simulations unless all NaCl is removed from the system, inducing a reopening of the outer and inner bottleneck. Our findings suggest that TolC is locked only on the periplasmic side in a sodium-dependent manner.

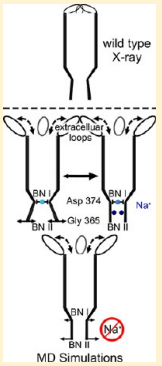

A member of the outer membrane efflux protein (OEP) family, TolC is a channel protein in the outer membrane of *Escherichia coli*[1,2] facilitating the transport of various toxic molecules.[3,4] Playing a major role in the expulsion of antibiotics[5,6] and the secretion of cell toxins,[7−9] TolC is highly versatile, functioning in conjunction with inner membrane transporters of the ATP binding cassette (ABC), resistance nodulation division (RND), or major facilitator (MF) type.[10−12] Interaction of the inner membrane transporter and outer membrane efflux duct is mediated by specialized periplasmic adaptor or membrane fusion proteins anchored to the inner membrane.[13,14] A prominent example of a TolC-dependent transport system is the AcrAB-TolC multidrug efflux pump employing the energy of a proton gradient over the inner membrane to power the expulsion of a broad range of substrates from the cell.[11] Although predominantly involved in substrate export, TolC is also known to be used as a backdoor by cell toxins like colicins to penetrate the outer membrane.[15,16]

Whereas channels like the cell toxin α-hemolysin, whose individual and unfolded subunits are also exported through TolC,[2] are constantly open, TolC access is regulated with the protein occurring in at least two states permitting or blocking the passage of substrates.[1,2] The details of the underlying gating mechanism are not fully understood.[2] The first crystal structure of the wild-type protein[17] revealed that TolC is a homotrimer, resembling the shape of a hollow cylinder organized in three domains. From a membrane-embedded β-barrel, cooperatively formed by all three monomers, an α-helical domain extends ∼100 Å into the periplasmic space surrounded in its middle section by the ringlike structure of an α/β equatorial domain.[1,2] TolC access was found to be restricted on both ends with three extracellular loops oriented toward the center of the β-barrel, limiting access to the channel to compounds with diameters of <7−8 Å in the wild type[17,18] and 7.2−10 Å in the mutant X-ray structures.[19,20] On the periplasmic side, the dense packing of the tip regions of 12 α-helices constricts the TolC channel to a diameter of ∼4.4 Å in the wild type[17,18] and 4−7.8 Å in the mutant crystal structures.[19,20] Whereas the occurrence of gating on the extracellular side is unclear,[17−21] combined mutagenesis−conductance experiments[22,23] and subsequent wild-type[18] and mutant TolC crystal structures[19,20] indicated the existence of two periplasmic bottlenecks: an inner bottleneck (BNI) at Asp371 and Asp374 where the binding of TolC-blocking hexaamminecobalt occurs[18,23] and an outer bottleneck (BNII) at Tyr362 and Arg367 involved in inter- and intramonomeric hydrogen bonds and salt bridges stabilizing a closed conformation.[22] Single and double mutations of these residues lead to increased ion conductance[22] as well as crystal structures showing partial symmetric[20] and asymmetric[19] opening toward the periplasm (Table 1).

Computational studies of TolC focused on molecular dynamics (MD) simulations comparing the wild type and BNII mutants,[21,24] as well as elastic network normal-mode analyses exploring possible opening mechanisms.[25] In a 20 ns MD study of wild-type and Tyr362Phe/Arg367Ser TolC, the mutant was reported to exhibit heightened flexibility in the periplasmic mouth region, while for the extracellular loops, a

Received: December 9, 2011
Revised: February 3, 2012
Published: February 6, 2012

dx.doi.org/10.1021/bi201814s | *Biochemistry* 2012, 51, 1719−1729

Table 1. TolC Opening States As Observed in the Crystal Structures and Our Molecular Dynamics Simulations

TolC structure	no. of extracellular loops closed[b]	outer periplasmic bottleneck Gly365 (BNII)		inner periplasmic bottleneck Asp374 (BNI)	
		avg TCA[a] (Å^2)	avg Cα distance (Å)	avg TCA (Å^2)	avg Cα distance (Å)
X-ray					
1EK9, wild type[17]	3	64.4	12.2	58.6	11.6
2VDD, Y362F/R367E[19]	0	203.8	21.8	76.7	13.8
2VDE, Y362F/R367E[19]	2	202.1	21.6	71.2	13.8
2WMZ, R367S[20]	0	154.8	18.9	65.7	12.3
2XMN, Y362F/R367S[20]	0	195.6	21.3	99.5	15.2
1TQQ, wild-type-bound hexaamminecobalt	3	61.3	11.9	64.6	12.2
simulation					
unmodified, BNII open	0–3	195.1 ± 42.6 (maximum of 334.8)	21.6 ± 3.4 (maximum of 31.3)	64.4 ± 8.2 (maximum of 98.4)	12.3 ± 1.1 (maximum of 17.3)
unmodified, BNII closed	0–2	32.0 ± 17.7 (minimum of 0.9)	11.7 ± 1.6 (minimum of 3.3)	58.7 ± 7.4 (minimum of 40.2)	11.7 ± 1.2 (minimum of 8.3)
modified, −4 Na, BNII closed	1–3	19.3 ± 7.9 (minimum of 0.9)	10.7 ± 1.2 (minimum of 3.3)	64.7 ± 6.7 (minimum of 46.0)	12.3 ± 0.6 (minimum of 9.0)
modified, no NaCl, BNII closed, I and II reopening	2	66.8 ± 31.7 (maximum of 133.5)	14.4 ± 2.5 (maximum of 25.6)	88.7 ± 11.6 (maximum of 125.3)	14.4 ± 0.9 (maximum of 19.3)

[a]TCA is the triangular cross-sectional area. [b]As closed as or closer than 1EK9 with $\theta \leq 90°$.

gating function was proposed on the basis of the observed closing motions.[21] Another study compared wild-type, Tyr362Phe/Arg367Glu, and Tyr362Phe/Arg367Asp TolC in a series of 20–30 ns MD simulations reporting wild-type-like closed periplasmic mouth conformations stabilized by potassium ions coordinated by Thr152, Asp153, and Glu/Asp367 in the mutant structures. Only when the potassium binding sites were emptied using an outer electric field was a BNII opening trend observed.[24] Beyond TolC, other multidrug efflux pump components have also recently been investigated computationally.[26–32]

Addressing the questions of extracellular access control and periplasmic gating mechanism, we performed nine independent, unbiased MD simulations of membrane-embedded wild-type TolC in a 150 mM NaCl solution sampling TolC conformational dynamics on a 150–300 ns time scale. Opening and closing freely on the extracellular side, TolC opens in the BNII region on the periplasmic side until the successive binding of two sodium ions preferably interacting with Asp371, Thr366, Thr368, and Asp153 induces closure. The resulting BNII conformation is more closed than any of the available crystal structures. Concurrent with a third site of heightened sodium residence probability at Asp374, TolC remains closed in the BNI region unless the removal of all NaCl from the system induces an opening response of BNI followed by a reopening of BNII. Displaying a so far unreported high degree of conformational dynamics in the channel mouth regions, our findings suggest that TolC is locked only on the periplasmic side in a sodium-dependent manner.

EXPERIMENTAL PROCEDURES

Molecular Dynamics Simulations. MD simulations were performed employing GROMACS version 4.0.3[33,34] and the GROMOS96-53a6 force field,[35] using the 1EK9 TolC crystal structure[17] as a starting structure. The protein was inserted in a pre-equilibrated 9.6 nm × 9.6 nm palmitoyloleoylphosphatidylethanolamine (POPE) bilayer patch[36] using INFLATEGRO.[37] The system was solvated with simple point charge water molecules[38] and 170 Na and 152 Cl ions, yielding a 150 mM NaCl solution and a total system charge of zero (Figure 1A).

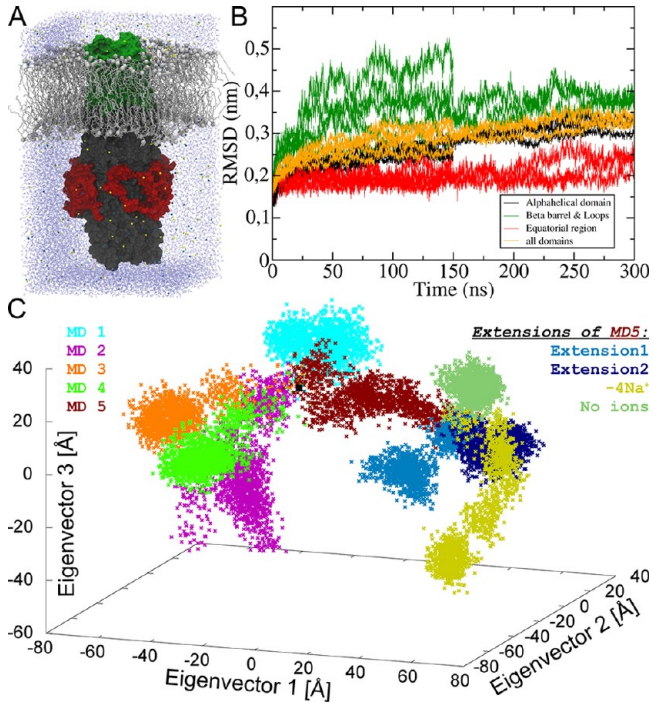

Figure 1. (A) Wild-type 1EK9 TolC was simulated in a POPE phospholipid/water environment at 150 mM NaCl. (B) As indicated by Cα root-mean-square deviations after respective least-squares alignment with the starting structure, the largest conformational changes occur in the region of the β-barrel and the extracellular loops. (C) Using the protein's α-carbons, TolC's path through conformational space in all simulations was mapped onto the first three eigenvectors in a principal component analysis.

Standard protonation states were assumed for titratable residues. After a 20 ns membrane equilibration with protein atoms position-restrained using a force constant of 1000 kJ mol^{-1} nm^{-2}, five independent MD runs with different starting velocities were performed, each 150 ns in length. Of these initial simulations, one was extended in four independent copies to 300 ns: two copies without any modifications, one

dx.doi.org/10.1021/bi201814s | Biochemistry 2012, 51, 1719–1729

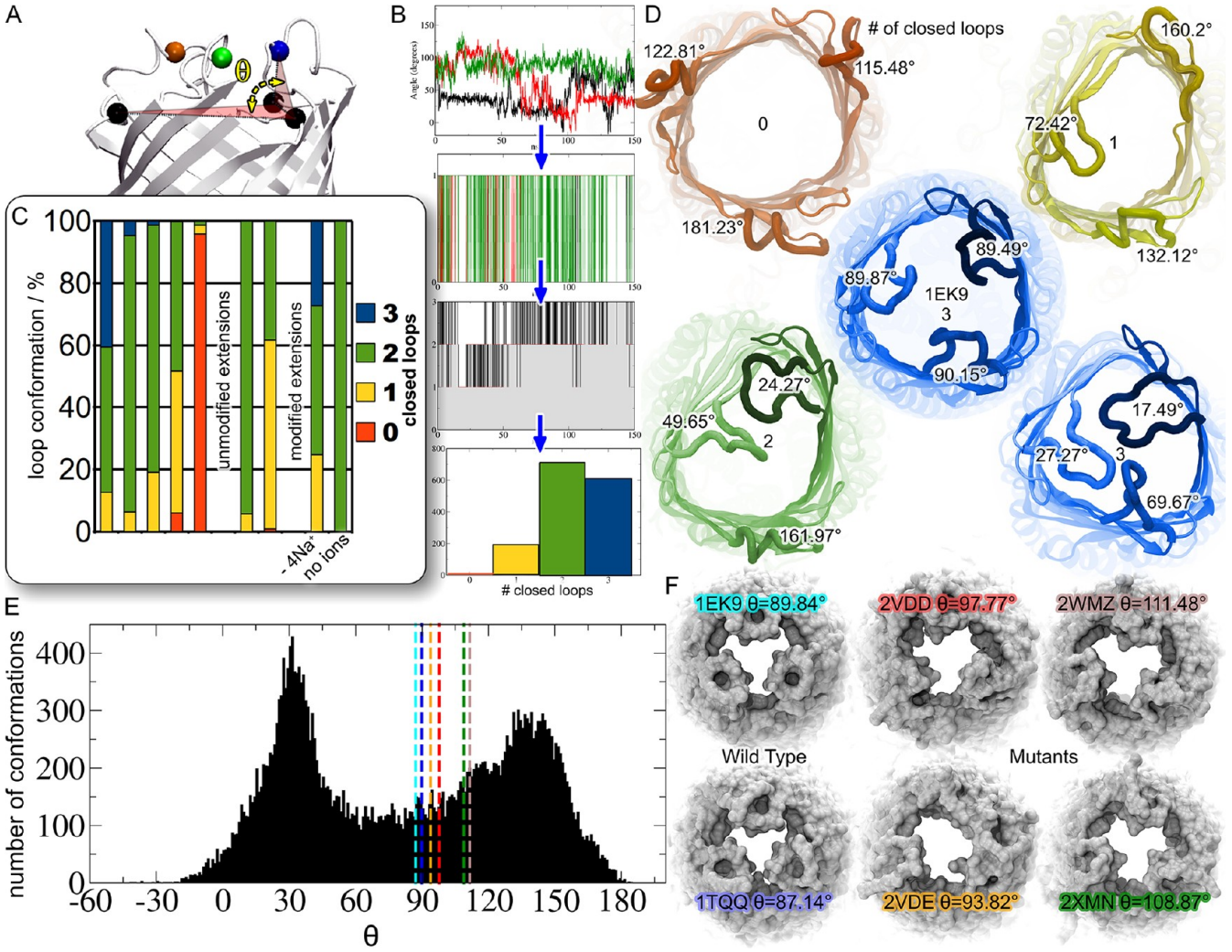

Figure 2. On the extracellular side, the TolC opening state was monitored using the dihedral angle θ defined by the α-carbons of Asp56 in the β-barrel and Ala270 in the tip of each extracellular loop. As the 1EK9 starting structure exhibits θ dihedrals of 89.8 ° (A), an extracellular loop was regarded closed or more closed than 1EK9 when θ was $\lesssim$90° (B). For each simulation, we calculated the number of closed extracellular loops and the percentage of simulation time spent in that conformation (C). Whereas TolC opens and closes throughout the simulations as illustrated by X-ray and simulation snapshots (D), partially open with one or two loops closed is the preferred conformation. As indicated by a θ histogram calculated over all unmodified simulations (E), the palette of extracellular loop conformations visited throughout our simulations exceeds the range of conformations observed in the known TolC X-ray structures (F).

copy with four Na ions removed, and one copy from which all NaCl ions had been deleted.

In the simulations, all bond lengths were constrained by LINCS[39] so that an integration time step of 2 fs could be chosen. Systems were simulated at 310 K, maintained separately for protein, lipids, and water by a Berendsen thermostat[40] with a time constant (τ_T) of 0.1 ps. Pressure coupling was done employing a Berendsen barostat[40] using a 1 bar reference pressure and a time constant of 4 ps. Semiisotropic pressure coupling was employed to permit bilayer fluctuations in the membrane plane. Electrostatic interactions were calculated using particle mesh Ewald (PME) summation,[41,42] and twin range cutoffs of 1.0 and 1.4 nm were applied for computing the van der Waals interactions.

Analysis. Similar to the analysis described in ref 24, the TolC opening state on the periplasmic side was monitored by calculating the triangular cross-sectional area (TCA) defined by the α-carbons of Asp374 and Gly365. On the extracellular side, the opening state was monitored through the dihedral angle θ spanned by the Cα atoms of Asp56 located in the β-barrel and Ala270 at the tip of each extracellular loop (Figure 2). As the outwardly closed 1EK9 crystal structure displays an average θ value of 89.8° (Figure 2A), an extracellular loop was regarded as closed as or more closed than 1EK9 whenever $\theta \leq 90°$. Conversely, a loop for which $\theta > 90°$ was considered more open than the 1EK9 X-ray structure. In each simulation, θ was monitored for each extracellular loop (Figure 2B, first panel) and subsequently converted to a binary representation of "more open" than 1EK9 (a value of 0) or "more closed" (assigned a value of 1) (Figure 2B, second panel). As a summary for each run, the number of loops in the closed conformation was determined (Figure 2B, third panel) and converted to a frequency histogram (Figure 2B, fourth panel) reflecting for each simulation the percentage occurrence of closed loop conformations (Figure 2C). To obtain an overview of the extracellular loop conformations visited throughout our simulations, we calculated a histogram showing the θ distribution in all unmodified runs (Figure 2E).

dx.doi.org/10.1021/bi201814s | Biochemistry 2012, 51, 1719–1729

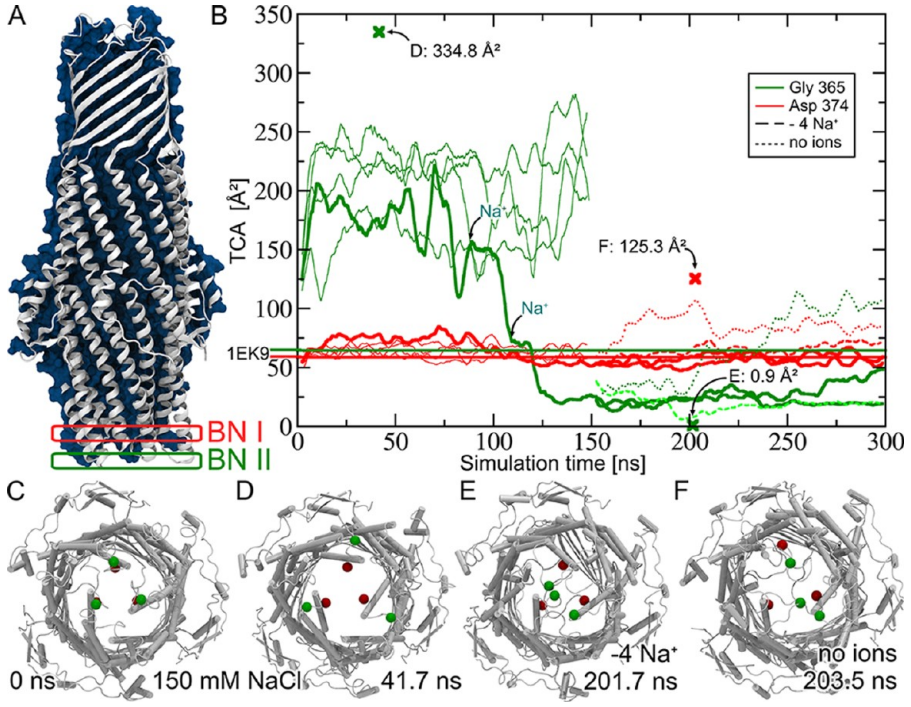

Figure 3. On the periplasmic side, the TolC opening state was monitored using the triangular cross-sectional area (TCA) spanned by the α-carbons of Asp374 and Gly365 representing the inner (BNI) and outer bottleneck region (BNII) (A). BNII visits open and closed conformations, with maximal closure occurring after a successive binding of two sodium ions (B). Simulation snapshots (C−F) illustrate periplasmic TolC conformations in the X-ray structure (C), at the maximal opening (D) and closure (E) of BNII at Gly396, and at the maximal opening of BNI, 53 ns after the removal of all NaCl from the system (F). For the sake of clarity, the TCAs have been smoothed using a running average filter of 5 ns. Bold crosses mark the unfiltered TCA maxima and minima corresponding to the simulation snapshots shown in panels D−F.

To analyze the distribution of sodium throughout the simulations, both one-dimensional (1D) Na density profiles along the membrane normal and average spatial sodium distributions were computed. The former was done using the GroMACS tool *g_density*, and for the latter, we employed the VolMap function in VMD version 1.9[43] using a spatial resolution of 1 Å^3 to analyze the distribution of sodium in the periplasmic bottleneck region at five density levels ranging from 0.01 to 0.6 Na/Å^3. Sodium binding and unbinding were monitored analyzing the *Z*-coordinate trajectory of each Na ion and computing for each TolC monomer the percentage of simulation time a residue of the periplasmic mouth region (residues 134−158 and 352−374) comes into contact with at least one sodium ion in at least one monomer. For this analysis, we employed a residue−Na distance cutoff of ≤3 Å. Both the sodium distributions and the residue contact analyses were performed using time frames of (I) 1−150 ns for the four simulations during which the outer periplasmic bottleneck (BNII) was open, (II) 125−300 ns for the two simulations during which BNII was closed, and (III) 150−300 ns for the run during which BNII remained closed after removal of four Na ions from the bottleneck region.

As described in ref 26, simulation average structures were calculated using an iterative scheme of calculating the average conformation and realigning the trajectory to that average structure before computing a new average structure. This procedure was repeated until the average structure stopped changing.

RESULTS

Protein Stability and Conformational Sampling. To monitor protein stability and conformational sampling throughout the simulations, we computed for each run Cα root-mean-square deviations (rmsds) of the entire protein, the β-barrel with extracellular loops, the α-helical domains, and the equatorial domain after least-squares fitting to the α-carbons of the crystal structure (Figure 1B). With rmsds ranging from 3.5 to 5.1 Å, the largest conformational changes occur in the β-barrel−extracellular loop regions, whereas the smallest changes take place in the equatorial domains with rmsds between 2 and 2.5 Å. Both α-helical domains and the entire protein display intermediate rmsds of 3−3.5 Å. Within 300 ns, no stable rmsd plateau is reached. As is evident from the Cα-based principal component analysis (Figure 1C) in each simulation, TolC samples different regions of conformational space.

Gating. *Extracellular Side.* To analyze TolC's opening state on the extracellular side, we monitored the dihedral angle θ formed by the Cα atoms of Asp56 in the β-barrel and Ala270 at the tip of each extracellular loop (Figure 2). Using the 1EK9 starting structure's average θ dihedral of 89.8° as a reference, we determined the number of loop conformations as closed or more closed than the aforementioned crystal structure. Throughout our simulations, the extracellular loops adopt a variety of conformations (Figure 2C) ranging from zero to three loops in the closed conformation (Figure 2D). As indicated by the percentage occurrence of the number of closed loop conformations in each run, "partially open" with one or two loops closed is the preferred conformation in our simulation (Figure 2C). Ranging from −30° to 180° with two distinctive peaks at 30° and 135°, the histogram of θ distributions calculated for all unmodified simulations (Figure 2E) indicates that the range of θ dihedrals in our simulations exceeds the range of 87.1−111.5° observed in all known wild-type and mutant TolC crystal structures (Figure 2F).

dx.doi.org/10.1021/bi201814s | *Biochemistry* 2012, 51, 1719−1729

Periplasmic Side. On the periplasmic side, we monitored the TolC opening state by calculating the triangular cross-sectional area (TCA) spanned by the Cα atoms of Asp374 and Gly365 (Figure 3) representing the inner (BNI) and outer periplasmic bottleneck region (BNII) (Figure 3A). In all runs, BNII opens within 10 ns with the TCA subsequently fluctuating around 195 ± 43 Å^2 (Figure 3B and Table 1). Concurrent with the successive binding of two sodium ions, in one simulation the TCA decreases in two steps below the 1EK9 crystal structure's TCA of 64.4 Å^2 (Table 1), reaching a new average plateau of 32 ± 18 Å^2 in the two unmodified extensions (Figure 3B, bold dark green lines, and Table 1) and 19 ± 8 Å^2 in the extension where four sodium ions were removed from the bottleneck regions (Figure 3B, dashed green line, and Table 1).When all NaCl is removed from the system, the TCA increases again, reaching 105 Å^2 by the end of the simulations (Figure 3B, dotted green line). With average BNI TCAs of 64 ± 8 Å^2 (BNII open) and 59 ± 7 Å^2 (BNII closed) in the unmodified simulations (Figure 3B, bold red line, and Table 1) and 65 ± 7 Å^2 after the removal of four Na atoms from the bottleneck region (Figure 3B, dashed red line, and Table 1), the inner bottleneck remains closed displaying a TCA similar to that of the 1EK9 X-ray structure except for the NaCl-free extension: here the TCA increases to 125 Å^2, settling at 80 Å^2 by the end of the simulations (Figure 3B, dotted red line). Whereas Figure 3C shows the conformation of BNI and BNII in the crystal structure, panels D−F of Figure 3 are simulation snapshots illustrating the maximal (Figure 3D) and minimal BNII opening (Figure 3E) of 334 and 0.9 Å^2, respectively (Table 1), as well as a maximal BNI opening of 125 Å^2 after the complete removal of NaCl (Figure 3F and Table 1).

Sodium Distributions. To determine the distribution of sodium ions and check for potential binding sites, we calculated 1D Na density profiles along the *Z*-axis (Figure 4A) and computed average spatial Na density distributions focusing on sodium in the periplasmic bottleneck regions (Figure 4B−D). Computed separately for the open and closed BNII conformations, the results were averaged over the respective runs using time frames of 0−150 ns (BNII open), 125−300 ns (BNII closed), and 150−300 ns (BNII closed after the removal of four Na atoms from the bottleneck region). As indicated by the peaks in the sodium density profile (Figure 4A), two preferred Na residence sites become apparent: the lipid headgroups and the region of the periplasmic bottlenecks where the density maximum is most pronounced in the unmodified simulations when BNII is closed. Zooming in on the bottleneck region, we find a heightened three-dimensional Na density near Asp374 and Asp371 exceeding 0.1 Na/Å^3 regardless of whether BNII is open (Figure 2B) or closed (Figure 2C,D). When BNII is closed, three density maxima become apparent in the unmodified runs (Figure 2C): two distinctive ones exceeding 0.6 Na/Å^3 at Asp371, Thr368, Thr366, and Asp153 and a smaller one between 0.2 and 0.3 Na/Å^3 near Asp374. When BNII is closed and four sodium ions are removed from the bottleneck region (Figure 2D), the 0.1 Na/Å^3 density is more smeared out and the former maxima are less pronounced.

Sodium Binding. Monitoring the *Z*-trajectories of all sodium ions in the system, we find that next to the lipid headgroup region an additional sodium trace becomes apparent near 14 nm, forming after 100 ns and remaining stable until the end of the simulations (Figure 5A). Zooming in on this region, we find that starting at 94 ns in the unmodified simulations the

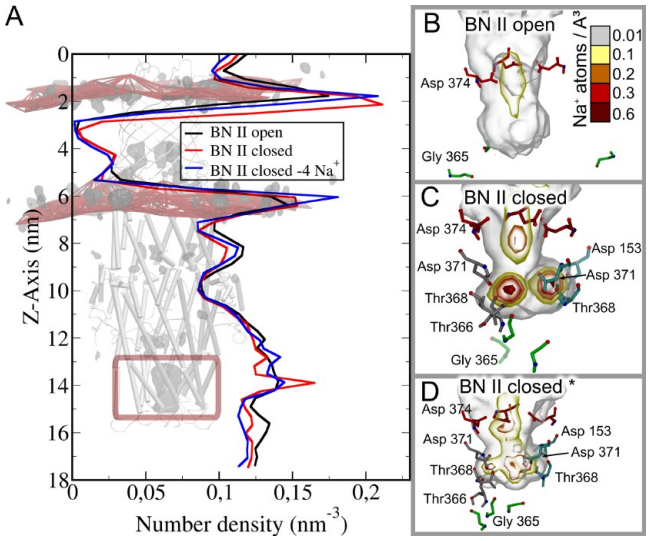

Figure 4. As indicated by partial sodium densities (A) calculated over all simulations where the outer bottleneck BNII is open (black) or closed during the unmodified runs (red) or after removal of the initially bound sodium ions (blue), there are two preferred sodium binding sites: at the lipid headgroups and between BNI and BNII. Spatial sodium density distributions in this area (B−D) indicate that Na densities exceeding 0.01 Na/Å^3 (transparent white isosurfaces) are present regardless of whether BNII is open or closed (B−D). When BNII is closed and the simulation system is unmodified, two distinctive maxima of Na density are present at Asp371, Thr368, Thr366, and Asp153, suggesting distinctive interaction sites (C). A third maximum of smaller density occurs near Asp374. After the removal of four sodium ions from the bottleneck regions, the 0.1 Na/Å^3 density is more smeared out and the former maxima are less pronounced (D). However, the reoccurrence of maximal sodium densities in this region suggests an immediate reoccupation of the interaction sites.

sodium trace is at first formed by single Na ions (Figure 5B,C), whereas after 120 ns, two Na ions contribute simultaneously to the trace with individual sodium residence times ranging up to 180 ns. In the simulation where all (four) sodium ions have been removed from the periplasmic bottleneck region after 150 ns, the sodium trace reappears after 5 ns (Figure 5D). During the remaining 145 ns of simulation time, single-ion occupancy is predominant and individual Na residence times do not exceed 30 ns. Via comparison of the Na trajectories with the BNII closure observed in the TCA analysis (Figure 3), it becomes evident that the binding of the first stable sodium at 94 ns precedes the first decrease in TCA in BNII closure by 8 ns, whereas the binding of the second sodium at 118 ns is concurrent with the beginning of the second decrease in TCA completing BNII closure.

To determine which residues are involved in sodium binding, we calculated for all residues in the periplasmic tip region their frequency of sodium contact (Figure 5E). Exceeding in at least one monomer 15% of observation time, Asp371, Thr366, Thr368, Asp153, and Asp 374 were identified as main sodium interaction sites with ion residence times ranging from 20 to 82%. Whereas Asp374 showed in all simulations similar Na contact times in all monomers, the other residues display an asymmetry in Na interaction characterized by Na residence times clearly higher in one monomer than in the other two.

Simulation versus X-ray. Throughout our simulations, wild-type TolC adopts conformations on the extracellular and periplasmic side that have not been reported in the published

dx.doi.org/10.1021/bi201814s | *Biochemistry* 2012, 51, 1719−1729

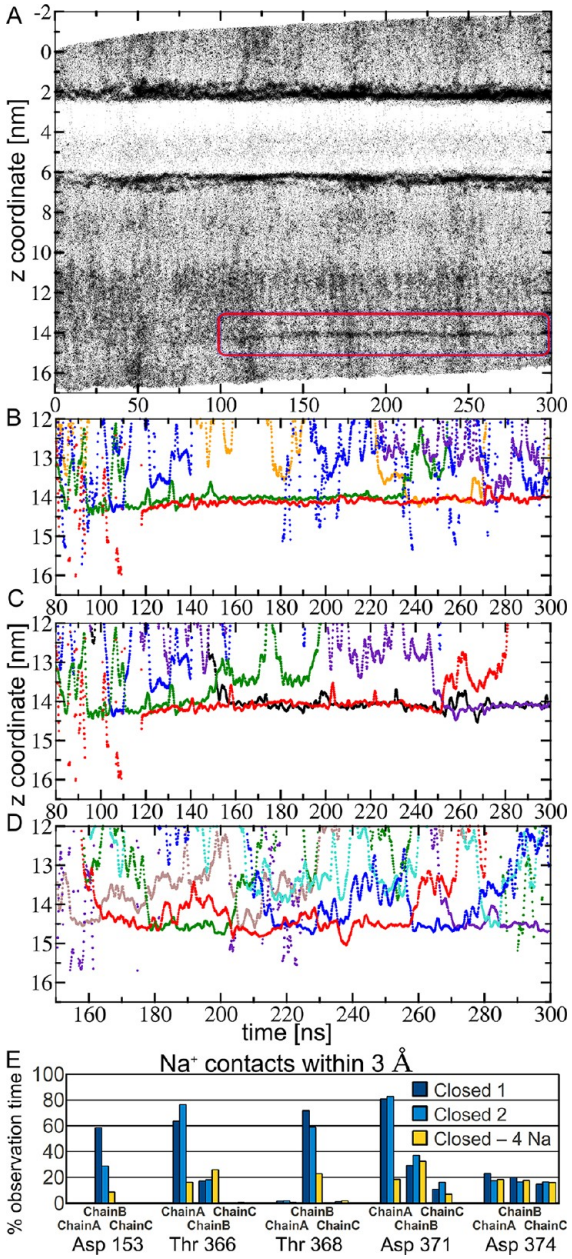

Figure 5. Sodium *Z*-trajectories (A–D) and frequency of Na residue contact (E). Monitoring the *Z*-coordinate of each sodium ion in the system, we find next to the lipid headgroups another preferred sodium residence site becomes apparent as indicated by a stable sodium trace near 14 nm forming after 100 ns (A). The following three panels are close-ups of this region showing individual sodium ions contributing to the stable Na trace in the unmodified simulations (B and C) and in the run following the removal of four Na ions from the bottleneck region after 150 ns (D). After 90 ns, at least one Na is present between 14 and 14.5 nm, whereas in the unmodified simulations after 120 ns, this region is preponderantly occupied by two Na ions (B and C) whose individual residence times range up to 180 ns. When Na is removed from the bottleneck region, the Na interaction region is reoccupied within 5 ns. Now, however, single-ion occupancy is predominant, and individual occupancy times are much shorter (D). Sodium-interacting residues exhibiting Na contacts of a minimum of 15% observation times in at least one monomer are summarized in panel E.

crystal structures.[17−20] To provide possible evidence explaining this discrepancy, we calculated the simulation average structure over all unmodified simulations and compared it to the 1EK9 crystal structure (Figure 6). As indicated by superimposition of the simulation average and X-ray structure after Cα least-squares fitting (Figure 6A) and calculation of Cα displacements for each monomer (Figure 6B), with an overall rmsd of 1.5 Å, the conformational differences are small and the largest deviations occur in the extracellular loops and the periplasmic tip region. Residues exceeding Cα displacements of 3 Å (highlighted in dark cyan in Figure 6C) partially coincide with 4 Å crystal contacts (van der Waals representation in Figure 6C) in the 1EK9 X-ray structure. Additionally, we have analyzed the *B* factors in all wild-type and mutant TolC X-ray structures and plotted their Cα root-mean-square fluctuations along the membrane normal (Figure S1 of the Supporting Information).

DISCUSSION

In this study, we report unbiased 150−300 ns MD simulations of wild-type TolC in a phospholipid/water environment in which TolC visits conformations on the extracellular and periplasmic side that have not been observed in any of the available wild-type and mutant TolC crystal structures.[17−20] We find TolC freely opening and closing on the extracellular side as well as in the region of the outer periplasmic bottleneck (BNII), monitored at Gly365, until the subsequent binding of two sodium ions interacting with Asp371, Thr366, Thr368, and Asp153 induces a closure resulting in a BNII conformation more closed than any of the available crystal structures. In the inner bottleneck (BNI) region at Asp374, TolC remains closed unless all NaCl is removed from the system, inducing an opening response of BNI followed by a reopening of BNII. We begin this section discussing the limitations of our approach and then proceed to our findings and their biological implications.

Limitations of Our Approach. As an outer membrane protein, TolC's microenvironment is characterized by a heterogeneous and asymmetric lipid composition containing lipolysaccharides in the outer leaflet, while the protein interacts with the peptidoglycan layer on the periplasmic side.[44] In our simulations, we approximated the outer membrane by a homogeneous POPE bilayer omitting a representation of the peptidoglycan layer. While it would certainly be desirable to have both components fully included in simulation studies, the development of the appropriate lipopolysaccharides and peptidoglycan molecular topologies is still in its infancy,[45−51] and at the time of writing, such simulation parameters were not yet available for *E. coli*. It will be interesting to see the influence these components have on the dynamics of outer membrane proteins especially because all crystallographic[17−20] and TolC conductance experiments[22,23] were conducted on the isolated protein. On the other hand, our choice of a simple uniform membrane model excluding the peptidoglycan is also justified by other simulation studies of outer membrane proteins making biologically relevant predictions using similar simplifications.[52−54] Whereas one could argue that the TolC behavior we observe on the extracellular side could be an artifact of our simplified membrane model, it is encouraging that one of the first lipopolysaccharide simulations studying outer membrane protein OprF[49] reported that the lipopolysaccharids have a stabilizing effect on the open conformation of the OprF extracellular loops that exhibit an architecture similar to that in TolC.

With any molecular dynamics study, the question of whether the simulated time has been sufficiently long with respect to the

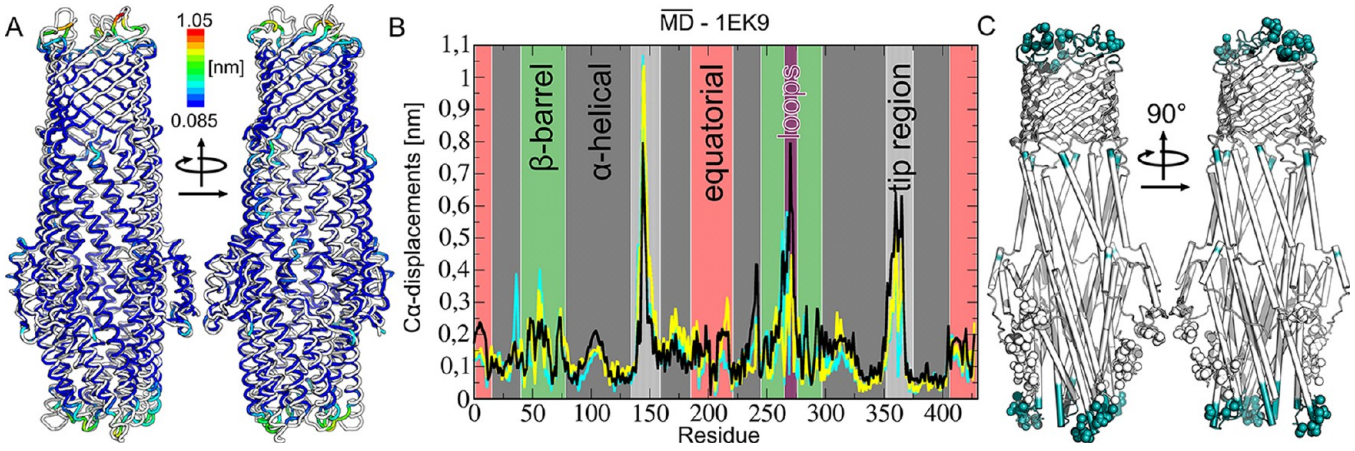

Figure 6. As indicated by the superposition of the 1EK9 X-ray structure (white) and TolC simulation average structure calculated over all unmodified simulations and colored by Cα displacement (A) and Cα displacements graphs for each monomer (B), the largest conformational differences occur in the extracellular loops and the periplasmic tip regions. The overall Cα rmsd between the simulation average and crystal structre is 1.5 Å. Residues exceeding Cα displacements of 3 Å (dark cyan) partially coincide with 4 Å crystal contacts (van der Waals representation) in the 1EK9 X-ray structure (C).

problem under investigation arises. Given the findings reported by Grossfield and Zuckerman[55] that 1.6 μs atomistic MD simulation of membrane-embedded rhodopsin was not enough for the protein structure to converge, our observations that TolC Cα rmsds are still increasing after 300 ns (Figure 1B), each run sampling different regions of conformational space (Figure 1C), and that the protein structure has therefore not equilibrated yet are not surprising, underscoring the need for long-time simulations as well as a careful restraint in using the term "equilibrated" when addressing protein structures in MD simulations. However, given that (a) our study's focus is on exploring wild-type TolC ground state dynamics near the crystal structure and (b) within the simulated time of 150−300 ns the protein already displayed unreported conformations (Figures 2 and 3) and ion interaction (Figures 4 and 5) both of which might provide potential new insights into the TolC functional mechanism (see below), we consider the amount of sampling achieved (Figure 1C) adequate for the purpose of this investigation, providing insights into wild-type TolC dynamics on a time scale that is 7.5−10 times longer than those of any previous TolC simulations.[21,24]

Simulation and X-ray. As summarized in Figure 7, throughout our simulations, wild-type TolC opens and closes on the extracellular (Figure 2) and periplasmic (Figure 3) side, adopting conformations that have not been reported in the wild-type[17,18] and mutant TolC crystal structures.[19,20] A possible explanation for why these conformations have not been detected yet could be that the crystal environment hinders the conformational changes we observe. Next to crystal type-dependent conformational differences of the same TolC mutant,[19] this hypothesis is supported by the distribution of 4 Å crystal contacts in the 1EK9 X-ray structure (Figure 6C), overlapping with residues where the conformational differences between the simulation average and crystal structure are maximal (Figure 6A,B). Furthermore, with an overall Cα rmsd of 1.5 Å, the conformational difference between the X-ray and simulation average structure is very small, suggesting that similar to the results in ref 56 the protein crystal could already contain the open and closed TolC conformations we observe in our simulations. In that case, these conformations either constitute only a minority of the total conformational ensemble

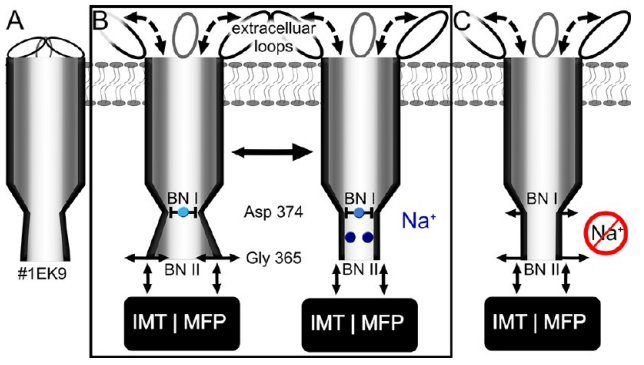

Figure 7. Whereas the available wild-type crystal structures restrict TolC access on both sides (A), throughout our simulations TolC opens and closes on the extracellular side. On the periplasmic side, the outer bottleneck BNII fluctuates around a conformation that is more open than the wild-type X-ray structures until the binding of two sodium ions induces a transition to a conformation that is more closed than in any of the known crystal structures. In both cases, the inner bottleneck BNI remains closed (B), unless all sodium is removed from the system, inducing a reopening of BNII and a beginning opening of BNI (C). If our simulations are correct, this observation could imply a locklike mechanism that is dependent on sodium or similar monovalent cations. Whereas the fluctuations of the outer bottleneck might play a role in the interaction with inner membrane transporters (IMT) or membrane fusion proteins (MFP), the principal accessibility from the extracellular side could hint at a novel mode of action for pharmaceutics specifically targeting the TolC interior.

in the 1EK9 crystal structure or on average are canceling each other out. Either way, the *B* factor maximum in the 100K wild-type TolC crystal structures[17,18] already implies a heightened degree of flexibility or crystal disorder in the extracellular loop region (Figure S1 of the Supporting Information).

Extracellular Access. Whereas the available structural[17−20] and computational data[21,24] suggest that TolC access is restricted on both sides, our findings imply that TolC gating occurs only on the periplasmic side (Figures 3 and 7) as TolC freely opens and closes on the extracellular side, suggesting here the absence of a gating mechanism in the isolated wild-type protein (Figures 2 and 7). The broad range of extracellular loop conformations visited throughout our simulations includes loop

Table 2. TolC Residues Affecting Conductance and Tertiary Structure and Involved in Ligand Binding

residue	single-channel conductance	X-ray crystallography	MD simulation
Thr152			part of the potassium binding pocket[24]
Asp153	D153A increases conductance[22]		part of the potassium binding pocket[24]
			high sodium binding affinity leads to a closure of BNII (this work)
Tyr362	Y362F increases conductance[22]	Y362F/R367E double mutants in 2VDD and 2VDE show an asymmetrically open BNII[19]	Y362F/R367S double mutant increases flexibility in the tip region[21]
		Y362F/R367S double mutants in 2VDD and 2VDE show a symmetrically open BNII[20]	
Thr366			high sodium binding affinity leads to a closure of BNII (this work)
Arg367	R367S increases conductance[22]	Y362F/R367E double mutants in 2VDD and 2VDE show an asymmetrically open BNII[19]	part of the potassium binding pocket[24]
		Y362F/R367S double mutants in 2VDD and 2VDE show a symmetrically open BNII[20]	Y362F/R367S double mutant increased flexibility in the tip region[21]
Thr368			high sodium binding affinity leads to a closure of BNII (this work)
Asp371	D371A increases conductance[23]	binding site for hexaamminecobalt[18]	high sodium binding affinity leads to a closure of BNII (this work)
Asp374	D374A increases conductance[23]	binding site for hexaamminecobalt[18]	high sodium binding affinity (this work)
		Asp374 ring as an indicator for BNI closure[20]	

orientations both more closed and more open (Figure 2D,E) than the available crystal structures[17−20] (Figure 2E,F). As indicated by the distribution of θ dihedral angles that we used to monitor the extracellular loops' opening state (Figure 2E), with θ values located between the two simulation maxima of 30° and 135°, the X-ray conformations represent only a small section of possible loop conformations. Whereas the crystal structures limit extracellular access to compounds with diameters of up to 7−8 Å in the wild-type[17,18] and 7.2−10 Å in the mutant crystal structures[19,20] (which we estimated by computing Connolly surfaces employing different probe sphere radii), we find that TolC accessibility is sterically only limited by the inner diameter of the β-barrel itself when all three loops are open (Figure 2D). If our simulations are correct, these results could either indicate the presence of additional regulation mechanisms in vivo or hint at the possibility of designing a novel group of TolC-directed drugs specifically targeting the protein interior. Possible experimental scenarios for testing the hypothesis of extracellular TolC accessibility could involve double-spin-label electron spin resonance spectroscopy measuring the distance between the tip regions of the extracellular loops or fluorescence spectroscopy experiments in which first a fluorescence dye-specific cross-linker is introduced into the TolC interior and then fluorescence activity is checked after external dye application, using dyes of different sizes, and protein extraction and purification. Beyond that, TolC-dependent colicin import[8,16] already provides evidence of the principal occurrence of an outwardly open conformation, and our findings might indicate that the extracellular entrance does not constitute a rate-limiting barrier in the colicin uptake process as wild-type TolC is capable of opening by itself. As we observe both opening and closing of the extracellular loops (Figure 2), our findings are also compatible with previous simulations[21,24] reporting extracellular closure. The fact that extracellular opening has not been reported in previous TolC simulations is likely due to the amount of conformational sampling achieved, which is larger in this study because of longer simulation times and the usage of multicopy MD.[26,56−59]

Periplasmic Access and a Sodium-Dependent Lock. Exhibiting an inner (BNI, monitored at Asp374)[23] and an outer periplasmic bottleneck (BNII, monitored at Gly365),[22] inwardly closed TolC has been shown by conductance experiments to be stabilized by inter- and intramonomeric hydrogen bonds and salt bridges.[22] Mutating residues involved in this network (Table 2) led to crystal structures more open than the wild type[19,20] (Table 1), whereas 20−30 ns MD simulations of the mutants reported increased flexibility of the periplasmic tip region,[21] potassium binding sites,[24] but no unforced opening of BNI or BNII.[21,24] Only when the effect of an outer electric field was simulated, accelerating cations toward the extracellular medium, could an opening of BNII be induced.[24] In our simulations, Na binding sites and spontaneous BNII opening and closure were observed in the wild-type protein without applying any biasing forces. However, as high-residence probability sodium binding sites were observed in only one simulation after 120 ns, the presence of potassium sites in wild-type TolC cannot be excluded on the basis of the available data. Furthermore, given that (a) the ionic and hydration radii of sodium lie between those of potassium and lithium,[60−62] for which a conductance-lowering effect was reported compared to potassium,[22] and (b) TolC−NaCl conductivity experiments have not been reported yet to the best of our knowledge, different K− and Na−TolC interactions cannot be excluded on the basis of the currently available data.

Although they display similar opening states in the wild-type crystal structures (Figure 3 and Table 1), BNI and BNII behave differently in our simulations. Whereas BNI remains closed unless all NaCl is removed from the system (Figure 3B), BNII occurs in two conformational states that have not been reported in previous wild-type X-ray structures or MD simulations (Figures 3 and 7 and Table 1). In the open state, BNII is more open than the wild type and comparably open compared to the mutant crystal structures (Table 1), whereas in the closed state, BNII is more closed than any of the available TolC crystal structures but still permits the passage of ions. Though open is the predominant state in our simulations, in one run we observe a spontaneous transition to closed state

BNII completed after 120 ns that is induced and subsequently stabilized by two sodium ions (Figure 3) interacting with residues located in a region where a network of hydrogen bonds and salt bridges has been identified as stabilizing inwardly closed TolC[19,20,22] (Figures 4 and 5 and Table 2). Closed BNII does not reopen during the following 180 ns unless all NaCl is removed from the system. In total, we find three preferred sodium residence sites (Figure 4B–D): two sharply defined ones with Na preferentially interacting with Asp371, Thr366, Thr368, and Asp153 of monomer A or B when BNII is closed and a less pronounced and centrally located site near Asp374 that does not show any monomer preference and is present regardless if BNII is open or closed (Figures 4 and 5).

If our simulations are correct, our findings of distinctive sodium interaction sites and the bottlenecks responding to the presence (BNII closure) or absence (opening of BNI and BNII) of sodium imply that periplasmic TolC access is restricted by a sodium-dependent lock. Whereas so far ion binding sites have been reported for only hexaamminecobalt[18] and potassium,[24] the presence of sodium binding sites in the bottleneck region is plausible given the high concentration of negative surface charges in this area,[17] as well as the location and preferred residue interaction of our proposed sodium sites overlapping with residues shown to be involved in stabilizing an inwardly closed TolC conformation[19,20,22] (Table 2). Furthermore, given that it is not uncommon that ion electron density is misinterpreted as water in the determination of X-ray crystallographic structures,[63] the presence of several water molecules in the region of our proposed sodium interaction sites in the wild-type 1EK9 crystal structure[17] could be interpreted as further evidence supporting our hypothesis, assuming some of the crystal water positions actually correspond to sodium.

Depending on whether the observed BNII closure is reversible without requiring further interaction partners, the sodium-dependent lock mechanism we propose would involve a single (BNI) or double bolt (BNII). Although closed state BNII remains stable for 180 ns throughout our simulations under unaltered (Figure 3B, bold lines) and modified (Figure 3B, dashed line) conditions, our results cannot exclude the reopening of BNII after, for example, 1800 ns. On the other hand, the increasing TCA observed during the last 50 ns in one of the unmodified extensions (Figure 3B, bold line) could indicate a beginning reopening of BNII, and the presence of only a single sodium trace instead of two (Figure 5B) supports a stabilizing sodium effect. However, as the question of whether BNII opens and closes freely cannot be decided on the basis of our current simulation data, further experiments to measure the periplasmic opening state in the Gly365 region using, for example, double-spin-label EPR spectroscopy are required. Whether sodium-induced BNII closure would be observable in electrophysiological conductance measurements, which to the best our knowledge have so far not been reported yet investigating the effect of NaCl on TolC conductivity, depends on (a) the lifetime of the BNII closed state, (b) the difference in Na flow (BNII closure in our simulations only slows ion flow but does not lead to a full blockage) and whether that difference is detectable in conductance experiments, and (c) the effect of the voltage used in the measurements and if the presence of an outer electric field hinders Na binding.

Whereas the absence of open and closed state BNII conformations in wild-type crystal structures[17,18] and simulation studies[21,24] could be explained as an effect of the crystal environment and the amount of conformational sampling as discussed above, plausible functional interpretations are conceivable for both fluctuating open state BNII and closed state BNII with regard to the interaction of TolC with its target proteins. The graspinglike motions of open state BNII (Figure 7B, left) could be interpreted as a first stage of initiating contact with the inner membrane transporter or membrane fusion protein, whereas closed state BNII (Figure 7B, right) could be relevant when TolC couples to an already assembled CusBA-like transporter–membrane fusion protein complex[64] in which the outer membrane efflux duct has to slide into the hoselike arrangement of membrane fusion proteins to complete the assembly of the entire pump, regardless of whether direct interaction occurs between the outer membrane efflux duct and the inner membrane transporter.

Displaying a continuously heightened sodium residence probability near Asp374 (Figures 4B–D and 7B) and a consistently X-ray-like closed conformation in all runs unless complete NaCl removal induces a so far unreported opening of first BNI and then BNII (Figures 3 and 7C and Table 1), BNI could constitute a bolt in our proposed sodium-dependent lock mechanism regardless of whether BNII opens and closes freely. Further underscoring the crucial role of the aspartate ring region in TolC gating,[18,23] our findings could be interpreted as showing that in vivo complex formation of TolC with its respective inner membrane transporter and membrane fusion protein induces conditions in the periplasmic TolC interior that hinder prolonged sodium interaction in the observed Asp374 region contributing to the unlocking of TolC. Without sodium, the three presumably deprotonated carboxyl groups of Asp374 would repel each other, inducing a sequential opening of BNI and BNII as observed in the NaCl-free simulation. Although this result could also imply an involvement of chloride in stabilizing an inwardly closed TolC conformation, the absence of any preferred interaction sites speaks against a chloride involvement. Whereas TolC conductance studies in the presence and absence of sodium could provide experimental evidence to test the hypothesis of a sodium-dependent lock, computer simulations of TolC in the presence of the inner membrane transporter or membrane fusion protein could yield insights into the involvement of the other components in the TolC opening mechanisms. MD simulations of TolC in presence of the isolated AcrB docking domain and the entire AcrB–AcrA complex are currently underway in our lab. Whereas we observe TolC opening motions on the periplasmic side, our data so far do not provide enough evidence to decide if periplasmic TolC opening occurs in a symmetrical[20] or asymmetrical manner.[19] However, the observation of two sodium interaction sites preferentially interacting only with two monomers of the TolC trimer (Figure 5E) could be interpreted as favoring the asymmetric opening hypothesis. Either way, one should keep in mind the possibility that the different opening conformations observed crystallographically[19,20] could simply represent two states of the same process.

CONCLUSIONS

Conducting a series of independent, unbiased 150–300 ns MD simulations of wild-type TolC in a phospholipid membrane/150 mM NaCl water environment, we find that TolC opens and closes freely on the extracellular side, suggesting the absence of a gating mechanism on this side in the isolated protein. On the periplasmic side, we observe the outer

periplasmic bottleneck region adopting in all simulations a conformation more open then the TolC wild-type crystal structures until in one run the successive binding of two sodium ions induces the transition to a conformation more closed than any of the available TolC X-ray structures. Concurrent with a heightened sodium residence probability near Asp374, the inner periplasmic bottleneck region at Asp374 remains closed throughout the simulations unless all NaCl is removed from the system, inducing a reopening of outer and inner bottlenecks. Our findings suggest that TolC is locked only on the periplasmic side in a sodium-dependent manner.

■ ASSOCIATED CONTENT

Supporting Information

A supporting figure. This material is available free of charge via the Internet at http://pubs.acs.org.

■ AUTHOR INFORMATION

Corresponding Author

*E-mail: kandt@bit.uni-bonn.de. Phone: 49 228 2699 324. Fax: 49 228 2699 341.

Funding

This work was financially supported by the Ministerium für Innovation, Wissenschaft and Forschung des Landes Nordrhein-Westfalen. C.K. is a junior research group leader funded by the NRW Rückkehrerprogramm.

Notes

The authors declare no competing financial interest.

■ ACKNOWLEDGMENTS

We thank Nadine Fischer and Thomas H. Schmidt for proofreading and helpful comments.

■ REFERENCES

(1) Koronakis, V., Eswaran, J., and Hughes, C. (2004) Structure and function of TolC: The bacterial exit duct for proteins and drugs. *Annu. Rev. Biochem. 73*, 467−489.

(2) Zgurskaya, H. I., Krishnamoorthy, G., Ntreh, A., and Lu, S. (2011) Mechanism and Function of the Outer Membrane Channel TolC in Multidrug Resistance and Physiology of Enterobacteria. *Front. Microbiol. 2*, 189.

(3) Benz, R., Maier, E., and Gentschev, I. (1993) TolC of *Escherichia coli* functions as an outer membrane channel. *Zentralbl. Bakteriol. 278*, 187−196.

(4) Fralick, J. A. (1996) Evidence that TolC is required for functioning of the Mar/AcrAB efflux pump of *Escherichia coli*. *J. Bacteriol. 178*, 5803−5805.

(5) Fralick, J. A., and Burns-Keliher, L. L. (1994) Additive effect of tolC and rfa mutations on the hydrophobic barrier of the outer membrane of *Escherichia coli* K-12. *J. Bacteriol. 176*, 6404−6406.

(6) Sulavik, M. C., Houseweart, C., Cramer, C., Jiwani, N., Murgolo, N., Greene, J., DiDomenico, B., Shaw, K. J., Miller, G. H., Hare, R., and Shimer, G. (2001) Antibiotic susceptibility profiles of *Escherichia coli* strains lacking multidrug efflux pump genes. *Antimicrob. Agents Chemother. 45*, 1126−1136.

(7) Delgado, M. A., Solbiati, J. O., Chiuchiolo, M. J., Farias, R. N., and Salomon, R. A. (1999) *Escherichia coli* outer membrane protein TolC is involved in production of the peptide antibiotic microcin J25. *J. Bacteriol. 181*, 1968−1970.

(8) Hwang, J., Zhong, X., and Tai, P. C. (1997) Interactions of dedicated export membrane proteins of the colicin V secretion system: CvaA, a member of the membrane fusion protein family, interacts with CvaB and TolC. *J. Bacteriol. 179*, 6264−6270.

(9) Wandersman, C., and Delepelaire, P. (1990) TolC, an *Escherichia coli* outer membrane protein required for hemolysin secretion. *Proc. Natl. Acad. Sci. U.S.A. 87*, 4776−4780.

(10) Moussatova, A., Kandt, C., O'Mara, M. L., and Tieleman, D. P. (2008) ATP-binding cassette transporters in *Escherichia coli*. *Biochim. Biophys. Acta 1778*, 1757−1771.

(11) Nikaido, H. (2011) Structure and mechanism of RND-type multidrug efflux pumps. *Adv. Enzymol. Relat. Areas Mol. Biol. 77*, 1−60.

(12) Saier, M. H., and Paulsen, I. T. (2001) Phylogeny of multidrug transporters. *Semin. Cell Dev. Biol. 12*, 205−213.

(13) Dinh, T., Paulsen, I. T., and Saier, M. H. Jr. (1994) A family of extracytoplasmic proteins that allow transport of large molecules across the outer membranes of Gram-negative bacteria. *J. Bacteriol. 176*, 3825−3831.

(14) Zgurskaya, H. I. (2009) Multicomponent drug efflux complexes: Architecture and mechanism of assembly. *Future Microbiol. 4*, 919−932.

(15) Cascales, E., Buchanan, S. K., Duche, D., Kleanthous, C., Lloubes, R., Postle, K., Riley, M., Slatin, S., and Cavard, D. (2007) Colicin biology. *Microbiol. Mol. Biol. Rev. 71*, 158−229.

(16) Zakharov, S. D., Eroukova, V. Y., Rokitskaya, T. I., Zhalnina, M. V., Sharma, O., Loll, P. J., Zgurskaya, H. I., Antonenko, Y. N., and Cramer, W. A. (2004) Colicin occlusion of OmpF and TolC channels: Outer membrane translocons for colicin import. *Biophys. J. 87*, 3901−3911.

(17) Koronakis, V., Sharff, A., Koronakis, E., Luisi, B., and Hughes, C. (2000) Crystal structure of the bacterial membrane protein TolC central to multidrug efflux and protein export. *Nature 405*, 914−919.

(18) Higgins, M. K., Eswaran, J., Edwards, P., Schertler, G. F., Hughes, C., and Koronakis, V. (2004) Structure of the ligand-blocked periplasmic entrance of the bacterial multidrug efflux protein TolC. *J. Mol. Biol. 342*, 697−702.

(19) Bavro, V. N., Pietras, Z., Furnham, N., Pérez-Cano, L., Fernández-Recio, J., Pei, X. Y., Misra, R., and Luisi, B. (2008) Assembly and channel opening in a bacterial drug efflux machine. *Mol. Cell 30*, 114−121.

(20) Pei, X. Y., Hinchliffe, P., Symmons, M. F., Koronakis, E., Benz, R., Hughes, C., and Koronakis, V. (2011) Structures of sequential open states in a symmetrical opening transition of the TolC exit duct. *Proc. Natl. Acad. Sci. U.S.A. 108*, 2112−2117.

(21) Vaccaro, L., Scott, K. A., and Sansom, M. S. P. (2008) Gating at both ends and breathing in the middle: Conformational dynamics of TolC. *Biophys. J. 95*, 5681−5691.

(22) Andersen, C., Koronakis, E., Bokma, E., Eswaran, J., Humphreys, D., Hughes, C., and Koronakis, V. (2002) Transition to the open state of the TolC periplasmic tunnel entrance. *Proc. Natl. Acad. Sci. U.S.A. 99*, 11103−11108.

(23) Andersen, C., Koronakis, E., Hughes, C., and Koronakis, V. (2002) An aspartate ring at the TolC tunnel entrance determines ion selectivity and presents a target for blocking by large cations. *Mol. Microbiol. 44*, 1131−1139.

(24) Schulz, R., and Kleinekathöfer, U. (2009) Transitions between closed and open conformations of TolC: The effects of ions in simulations. *Biophys. J. 96*, 3116−3125.

(25) Phan, G., Benabdelhak, H., Lascombe, M. B., Benas, P., Rety, S., Picard, M., Ducruix, A., Etchebest, C., and Broutin, I. (2010) Structural and dynamical insights into the opening mechanism of *P. aeruginosa* OprM channel. *Structure 18*, 507−517.

(26) Fischer, N., and Kandt, C. (2011) Three ways in, one way out: Water dynamics in the trans-membrane domains of the inner membrane translocase AcrB. *Proteins 79*, 2871−2885.

(27) Phan, G., Benabdelhak, H., Lascombe, M. B., Benas, P., Rety, S., Picard, M., Ducruix, A., Etchebest, C., and Broutin, I. (2010) Structural and dynamical insights into the opening mechanism of *P. aeruginosa* OprM channel. *Structure 18*, 507−517.

(28) Schulz, R., Vargiu, A. V., Collu, F., Kleinekathofer, U., and Ruggerone, P. (2010) Functional rotation of the transporter AcrB: Insights into drug extrusion from simulations. *PLoS Comput. Biol. 6*, e1000806.

(29) Schulz, R., Vargiu, A. V., Ruggerone, P., and Kleinekathofer, U. (2011) Role of water during the extrusion of substrates by the efflux transporter AcrB. *J. Phys. Chem. B 115*, 8278−8287.
(30) Vaccaro, L., Koronakis, V., and Sansom, M. S. (2006) Flexibility in a drug transport accessory protein: Molecular dynamics simulations of MexA. *Biophys. J. 91*, 558−564.
(31) Vargiu, A. V., Collu, F., Schulz, R., Pos, K. M., Zacharias, M., Kleinekathofer, U., and Ruggerone, P. (2011) Effect of the F610A mutation on substrate extrusion in the AcrB transporter: Explanation and rationale by molecular dynamics simulations. *J. Am. Chem. Soc. 133*, 10704−10707.
(32) Yao, X. Q., Kenzaki, H., Murakami, S., and Takada, S. (2010) Drug export and allosteric coupling in a multidrug transporter revealed by molecular simulations. *Nat. Commun. 1*, 117.
(33) Berendsen, H. J. C., Vanderspoel, D., and Vandrunen, R. (1995) Gromacs: A Message-Passing Parallel Molecular-Dynamics Implementation. *Comput. Phys. Commun. 91*, 43−56.
(34) Hess, B., Kutzner, C., van der Spoel, D., and Lindahl, E. (2008) GROMACS 4: Algorithms for highly efficient, load-balanced, and scalable molecular simulation. *J. Chem. Theory Comput. 4*, 435−447.
(35) Oostenbrink, C., Villa, A., Mark, A. E., and van Gunsteren, W. F. (2004) A biomolecular force field based on the free enthalpy of hydration and solvation: The GROMOS force-field parameter sets 53A5 and 53A6. *J. Comput. Chem. 25*, 1656−1676.
(36) Tieleman, D. P., and Berendsen, H. J. (1998) A molecular dynamics study of the pores formed by *Escherichia coli* OmpF porin in a fully hydrated palmitoyloleoylphosphatidylcholine bilayer. *Biophys. J. 74*, 2786−2801.
(37) Kandt, C., Ash, W. L., and Tieleman, D. P. (2007) Setting up and running molecular dynamics simulations of membrane proteins. *Methods 41*, 475−488.
(38) Berendsen, H. J. C., Postma, J. P. M., van Gunsteren, W. F., and Hermans, J. (1981) Interaction models for water in relation to protein hydration. *Intermol. Forces,*, 331−342.
(39) Hess, B., Bekker, H., Berendsen, H. J. C., and Fraaije, J. G. E. M. (1997) LINCS: A linear constraint solver for molecular simulations. *J. Comput. Chem. 18*, 1463−1472.
(40) Berendsen, H. J. C., Postma, J. P. M., Vangunsteren, W. F., Dinola, A., and Haak, J. R. (1984) Molecular-Dynamics with Coupling to an External Bath. *J. Chem. Phys. 81*, 3684−3690.
(41) Darden, T., York, D., and Pedersen, L. (1993) Particle Mesh Ewald: An N.Log(N) Method for Ewald Sums in Large Systems. *J. Chem. Phys. 98*, 10089−10092.
(42) Essmann, U., Perera, L., Berkowitz, M. L., Darden, T., Lee, H., and Pedersen, L. G. (1995) A Smooth Particle Mesh Ewald Method. *J. Chem. Phys. 103*, 8577−8593.
(43) Humphrey, W., Dalke, A., and Schulten, K. (1996) VMD: Visual molecular dynamics. *J. Mol. Graphics 14*, 27−38.
(44) Lugtenberg, B., and Van Alphen, L. (1983) Molecular architecture and functioning of the outer membrane of *Escherichia coli* and other Gram-negative bacteria. *Biochim. Biophys. Acta 737*, 51−115.
(45) Kotra, L. P., Golemi, D., Amro, N. A., Liu, G. Y., and Mobashery, S. (1999) Dynamics of the lipopolysaccharide assembly on the surface of *Escherichia coli*. *J. Am. Chem. Soc. 121*, 8707−8711.
(46) Lins, R. D., and Straatsma, T. P. (2001) Computer simulation of the rough lipopolysaccharide membrane of *Pseudomonas aeruginosa*. *Biophys. J. 81*, 1037−1046.
(47) Meroueh, S. O., Bencze, K. Z., Hesek, D., Lee, M., Fisher, J. F., Stemmler, T. L., and Mobashery, S. (2006) Three-dimensional structure of the bacterial cell wall peptidoglycan. *Proc. Natl. Acad. Sci. U.S.A. 103*, 4404−4409.
(48) Piggot, T. J., Holdbrook, D. A., and Khalid, S. (2011) Electroporation of the *E. coli* and *S. aureus* membranes: Molecular dynamics simulations of complex bacterial membranes. *J. Phys. Chem. B 115*, 13381−13388.
(49) Straatsma, T. P., and Soares, T. A. (2009) Characterization of the outer membrane protein OprF of *Pseudomonas aeruginosa* in a lipopolysaccharide membrane by computer simulation. *Proteins 74*, 475−488.
(50) Vollmer, W., and Bertsche, U. (2008) Murein (peptidoglycan) structure, architecture and biosynthesis in *Escherichia coli*. *Biochim. Biophys. Acta 1778*, 1714−1734.
(51) Vollmer, W., Blanot, D., and de Pedro, M. A. (2008) Peptidoglycan structure and architecture. *FEMS Microbiol. Rev. 32*, 149−167.
(52) Cuesta-Seijo, J. A., Neale, C., Khan, M. A., Moktar, J., Tran, C. D., Bishop, R. E., Pomes, R., and Prive, G. G. (2010) PagP crystallized from SDS/cosolvent reveals the route for phospholipid access to the hydrocarbon ruler. *Structure 18*, 1210−1219.
(53) Gumbart, J., Wiener, M. C., and Tajkhorshid, E. (2009) Coupling of calcium and substrate binding through loop alignment in the outer-membrane transporter BtuB. *J. Mol. Biol. 393*, 1129−1142.
(54) Hajjar, E., Bessonov, A., Molitor, A., Kumar, A., Mahendran, K. R., Winterhalter, M., Pags, J.-M., Ruggerone, P., and Ceccarelli, M. (2010) Toward Screening for Antibiotics with Enhanced Permeation Properties through Bacterial Porins. *Biochemistry 49*, 6928−6935.
(55) Grossfield, A., and Zuckerman, D. M. (2009) Quantifying uncertainty and sampling quality in biomolecular simulations. *Annu. Rep. Comput. Chem. 5*, 23−48.
(56) Kandt, C., Xu, Z., and Tieleman, D. P. (2006) Opening and closing motions in the periplasmic vitamin B12 binding protein BtuF. *Biochemistry 45*, 13284−13292.
(57) Caves, L. S., Evanseck, J. D., and Karplus, M. (1998) Locally accessible conformations of proteins: Multiple molecular dynamics simulations of crambin. *Protein Sci. 7*, 649−666.
(58) Das, B., Helms, V., Lounnas, V., and Wade, R. C. (2000) Multicopy molecular dynamics simulations suggest how to reconcile crystallographic and product formation data for camphor enantiomers bound to cytochrome P-450cam. *J. Inorg. Biochem. 81*, 121−131.
(59) Kandt, C., and Tieleman, D. P. (2010) Holo-BtuF stabilizes the open conformation of the vitamin B12 ABC transporter BtuCD. *Proteins 78*, 738−753.
(60) Cordero, B., Gomez, V., Platero-Prats, A. E., Reves, M., Echeverria, J., Cremades, E., Barragan, F., and Alvarez, S. (2008) Covalent radii revisited. *Dalton Trans.,*, 2832−2838.
(61) Nightingale, E. R. (1959) Phenomenological Theory of Ion Solvation: Effective Radii of Hydrated Ions. *J. Phys. Chem. 63*, 1381−1387.
(62) Shannon, R. D. (1976) Revised effective ionic radii and systematic studies of interatomic distances in halides and chalcogenides. *Acta Crystallogr. A32*, 751−767.
(63) Faust, A., Panjikar, S., Mueller, U., Parthasarathy, V., Schmidt, A., Lamzin, V. S., and Weiss, M. S. (2008) A tutorial for learning and teaching macromolecular crystallography. *J. Appl. Crystallogr. 41*, 1161−1172.
(64) Su, C. C., Long, F., Zimmermann, M. T., Rajashankar, K. R., Jernigan, R. L., and Yu, E. W. (2011) Crystal structure of the CusBA heavy-metal efflux complex of *Escherichia coli*. *Nature 470*, 558−562.